

Budget study of the internal variability in ensemble simulations of the Canadian Regional Climate Model at the seasonal scale

Oumarou Nikiema¹ and René Laprise¹

Received 25 February 2011; revised 11 May 2011; accepted 7 June 2011; published 24 August 2011.

[1] Previous investigations with nested regional climate models have revealed that simulations are sensitive to the initial conditions (IC). This results in internal variability (IV) in ensembles of simulations initialized with small differences in IC. In a previous study, a quantitative budget calculation has documented the physical processes responsible for the rapid growth of IV in simulations with the Canadian Regional Climate Model (CRCM). By using an ensemble of 20 simulations performed for the 1993 summer season, we extend the previous study to further our understanding about the physical processes responsible for the maintenance and fluctuations of IV in a seasonal simulation with CRCM. We have identified and quantified various terms in the prognostic budget equations of IV for the potential temperature and the absolute vorticity. For these studied variables, the covariance of fluctuations acting on the gradient of the ensemble mean of variables generally contributes to increasing the IV, indicating that the transport of heat and vorticity is down the gradient of ensemble mean potential temperature and absolute vorticity. The horizontal transport of IV by ensemble mean flow acts as a sink term, the IV transport out of the study domain contributing to reduce the IV. On average in the troposphere and at the seasonal scale, results confirm that there is no trend in IV although it greatly fluctuates in time. Our results also show that IV is a natural phenomenon arising from the chaotic nature of the atmosphere. In a time-averaged sense, the IV budget reduces to a balance between generation and destruction terms.

Citation: Nikiema, O., and R. Laprise (2011), Budget study of the internal variability in ensemble simulations of the Canadian Regional Climate Model at the seasonal scale, *J. Geophys. Res.*, 116, D16112, doi:10.1029/2011JD015841.

1. Introduction

[2] Because of their ability to simulate physical processes operating at fine spatial scales, high-resolution regional climate models (RCM) have been increasingly used to simulate various components of the Earth system at the regional scale, in order to understand the past and present climate, and to downscale future climate projections from Global Climate Models (GCM). Due to their limited area of integration, RCMs must be driven at their lateral boundaries by large-scale atmospheric variables; usually Lateral Boundary Conditions (LBC) are provided from either GCM simulation output or gridded analyses of observations.

[3] Previous studies with RCMs have shown that their simulations are sensitive to initial conditions (IC) due to the chaotic nature of the atmospheric system [Lorenz, 1967]. In fact, ensembles of RCMs' simulations launched from slightly different IC generate solutions of the atmospheric variables that become significantly different after a few days of simulation [Giorgi and Bi, 2000; Weisse et al., 2000;

Rinke and Dethloff, 2000; Christensen et al., 2001; Caya and Biner, 2004; Rinke et al. 2004; Lucas-Picher et al., 2004; Alexandru et al., 2007; de Elia et al., 2008; Lucas-Picher et al., 2008; Nikiéma and Laprise, 2010]. This sensitivity to IC is referred to as internal variability (IV), which can be quantified as the intermember spread in an ensemble of simulations run from different IC.

[4] Caya and Biner [2004] were among the first to study the IV using the Canadian RCM over a domain covering the eastern North America and a part of the Atlantic Ocean. They compared three 1 year simulations launched with different atmospheric and/or surface initial conditions; they found IV to be small in winter and to become much larger in summer. As noted by Giorgi and Bi [2000], the large IV in summer can be attributed to local and intermittent processes, such as convection and precipitation, whereas in winter, the stronger upper tropospheric flow sweeps away the generated IV. However, several studies suggest that, for a given season, the magnitude of IV strongly depends on domain size [Lucas-Picher et al., 2004, 2008; Alexandru et al., 2007].

[5] By using a set of 20 CRCM simulations, Alexandru et al. [2007] studied the 1993 summer season IV over eastern North America. The integrations shared exactly the same LBCs; the difference between them consisted only in a delay of 24 h at the beginning of two successive runs. Their results

¹Centre Étude et Simulation du Climat à l'Échelle Régionale, Université du Québec à Montréal, Montreal, Quebec, Canada.

showed that the IV magnitude strongly fluctuates with synoptic events during the simulations, and that the geographical distribution of IV differed between variables. They suggested that strong precipitation events in the southern United States appear to act as a triggering mechanism for the 850 hPa geopotential IV, which continues to develop along the storm track, reaching its maximum amplitude toward the northeast of the simulation domain.

[6] *Nikiema and Laprise* [2010] (hereinafter NL10) extended the work of *Alexandru et al.* [2007] in order to shed some light on the physical processes responsible of the episodic large growth of IV. They performed a quantitative diagnostic calculation to identify the various diabatic and dynamical contributions to the temporal variation and spatial distribution of IV. They established IV budget equations for the potential temperature and the relative vorticity. They showed that IV tendency arises from the contributions of four and eight main terms for the potential temperature and the relative vorticity, respectively. For these variables, the two IV budget equations consist of similar terms, notably terms relating to the transport of IV by ensemble mean flow and the covariance of fluctuations acting on the gradient of the ensemble mean state. They focused their analysis over a small period of interest characterized by rapid growth of IV. Their results show that IV maxima are found near the ground (925–1000 hPa) and the tropopause (200–300 hPa), with a minimum in the middle troposphere (600–700 hPa). The episodes of large growth of the IV are associated with strong synoptic events in the simulation, as mentioned by *Alexandru et al.* [2007]. They noted that the episodes of large decreases of IV occur when maxima of IV approach the northeast outflow boundary and are eventually transported out of the regional domain by the ensemble mean flow.

[7] The analysis of IV budget by NL10 revealed that the dominant terms responsible for the large increase of potential temperature IV are the covariance term involving the potential temperature fluctuations and diabatic heating fluctuations, and the covariance of intermember fluctuations acting upon ensemble mean gradients. Their study also suggested that the horizontal transport by the ensemble mean flow only contributes to the IV tendency during episodes of rapid decrease of IV, when they advect large IV pockets out of the regional domain. Finally, they found that, on average, the third-order terms have a negligible contribution, but they can be important when the IV becomes very large.

[8] The purpose of this study is to expand upon the work of NL10 with a special attention to the seasonal scale. By using the same 20 simulations of *Alexandru et al.* [2007], IV will be analyzed and compared to the transient-eddy variability (TV) for the 1993 summer. At the seasonal scale, we will quantify each contribution in the IV tendency equation over the whole troposphere. The paper is organized as follows. Section 2 will describe the 1993 summer ensemble of simulations, evaluation methods and IV budget equations for the potential temperature and the absolute vorticity. Results and analysis will follow in section 3 where we will examine and compare the IV and TV, and then we will analyze the vertical profile and time evolution of contributions to IV budget in order to quantify the 1993 summer

‘climatology’ of various contributions. The main conclusion will be summarized in section 4.

2. Data and Evaluation Methods

2.1. Domain and Simulation Data

[9] This study uses archived CRCM’s simulations described in detail by *Alexandru et al.* [2007] corresponding to 20-member simulations carried out on a 120 by 120 grid point computational domain. The study domain covers the eastern North America and part of the Atlantic Ocean [see *Alexandru et al.*, 2007, Figure 1]. In a nutshell, the CRCM (version 3.6.1) uses polar stereographic projection with a 45 km grid mesh (true at 60° latitude), 18 Gal-Chen levels in the vertical and a 15 min time step. The simulated fields were interpolated on the following set of prespecified pressure levels: 10, 20, 30, 50, 70, 100, 150, 200, 250, 300, 400, 500, 600, 700, 850, 925, 1000 and 1050 hPa. When the pressure is larger than the surface pressure, an extrapolation is made below the ground from the lowest model level. We mainly focused on the troposphere, i.e., the levels located between 250 and 1000 hPa. The fields were archived at 6-hourly intervals; atmospheric variables correspond to samples at archival time, whereas the source/sink terms correspond to cumulative contributions between archival times.

2.2. Climate Statistics of the Internal Variability

[10] As many preceding authors [e.g., *Alexandru et al.*, 2007; *Lucas-Picher et al.*, 2008; NL10], the present study calculates internal variability (IV) as the intermember spread in an ensemble of simulations, using the variance of departures from the ensemble mean:

$$\sigma_{\varphi}^2(i, j, k, t) = \frac{1}{N-1} \sum_{n=1}^N [\varphi_n(i, j, k, t) - \langle \varphi \rangle(i, j, k, t)]^2 \quad (1)$$

where $\varphi_n(i, j, k, t)$ refers to the value of variable φ on grid point (i, j) at level k at time t for member n in the N -member ensemble. The IV was computed in this way at all grid points and pressure levels and at each 6-hourly archived intervals. In the following, φ will refer either to potential temperature θ or absolute vorticity η . The operator $\langle \varphi \rangle$ refers to the ensemble mean of the variable φ_n defined as:

$$\langle \varphi \rangle = \frac{1}{N} \sum_{n=1}^N \varphi_n \quad (2)$$

where N represents the number of members in the ensemble of simulations.

[11] For comparison purpose, we will also present the transient-eddy variability (TV) that represents the natural variability of a meteorological field over time, mainly due to the weather systems traveling along the storm track [e.g., *Lucas-Picher et al.*, 2008]. The TV of a variable φ in simulation number n is calculated using the temporal variance $\hat{\sigma}_{\varphi_n}^2$ defined as [e.g., *Caya and Biner*, 2004]:

$$\hat{\sigma}_{\varphi_n}^2(i, j, k) = \frac{1}{\tau-1} \sum_{t=1}^{\tau} [\varphi_n(i, j, k, t) - \overline{\varphi_n(i, j, k)}]^2 \quad (3)$$

where $\overline{\varphi_n(i, j, k)^t}$ represents the time average of the variable over the season of interest and τ is the number of archive intervals in the season. The ensemble mean of the temporal variance $\langle \hat{\sigma}_\varphi^2 \rangle$ is used to obtain a more robust estimation of the natural variability in simulations.

[12] Different statistics were used to describe the IV temporal and spatial fluctuations. The time average of σ_φ^2 is used to evaluate the seasonal ‘climatology’ of the IV, defined as:

$$\overline{\sigma_\varphi^2}^t(i, j, k) = \frac{1}{\tau} \sum_{t=1}^{\tau} \sigma_\varphi^2(i, j, k, t) \quad (4)$$

[13] The vertical profile of the domain-averaged and seasonal averaged IV is obtained by using the domain average of $\overline{\sigma_\varphi^2}^t$, computed as:

$$\overline{\sigma_\varphi^2}^{XY}(k) = \frac{1}{I \times J} \sum_{i=1}^I \sum_{j=1}^J \overline{\sigma_\varphi^2}^t(i, j, k) \quad (5)$$

where I and J refer to the number of grid cells in the X and Y directions over the domain of interest. We neglect the map scale factor of the polar stereographic projection in the calculations. In practice the domain average was computed over a subdomain excluding the 10–grid point sponge zone and a 10–grid point spatial spin-up ribbon along the western lateral boundary.

[14] Finally, the vertical average of the seasonal IV is calculated as follows:

$$\overline{\sigma_\varphi^2}^p = \int_{p_T}^{p_B} \overline{\sigma_\varphi^2}^t dp / (p_B - p_T) \quad (6)$$

where p_T and p_B are the lowest and the highest pressure values in the vertical integral; in order to preserve the original unit of the field, the vertical integral has been divided by the difference between bottom and top pressure levels. In the following the vertical integral will be calculated with $p_T = 250$ hPa and $p_B = 1000$ hPa because our interest lies in the tropospheric region. A similar equation will also be used to compute the vertical average of the TV and each term in the IV budget equations.

2.3. Internal Variability Budget Equations

[15] In their study, NL10 established prognostic equations of the IV for two variables: potential temperature and relative vorticity. For each variable, they performed a quantitative diagnostic calculation to identify various diabatic and dynamical contributions to the temporal variation and spatial distribution of IV. They described in details the methodology used to establish the IV budget equations for these two atmospheric variables. In the polar stereographic and isobaric coordinates (X, Y, p), the IV equation of the potential temperature was established as:

$$L_\theta = R_\theta = A_h + A_v + B_h + B_v + C + E \quad (7)$$

where terms are given by:

$$L_\theta = \frac{\partial \sigma_\theta^2}{\partial t}$$

$$A_h = -\vec{\nabla} \bullet \langle \langle \vec{V} \rangle \sigma_\theta^2 \rangle; \quad A_v = -\frac{\partial \langle \langle \omega \rangle \sigma_\theta^2 \rangle}{\partial p}$$

$$B_h = -2 \langle \theta_n' \vec{V}_n' \rangle \bullet \vec{\nabla} \langle \theta \rangle; \quad B_v = -2 \langle \theta_n' \omega_n' \rangle \frac{\partial \langle \theta \rangle}{\partial p}$$

$$C = 2 \langle \theta_n' J_n' \rangle;$$

$$E = -2 \langle \theta_n' \vec{\nabla} \bullet \langle \theta_n' \vec{V}_n' \rangle \rangle - 2 \langle \theta_n' \frac{\partial}{\partial p} (\theta_n' \omega_n') \rangle$$

[16] The local change of the potential temperature variance (L_θ , referred to as the ‘‘left-hand side’’ term) results from the contribution of six main terms on the right-hand side (R_θ): (1) the horizontal (A_h) and vertical (A_v) transport terms that describe the convergence of the potential temperature IV by the ensemble mean flow; (2) the horizontal (B_h) and vertical (B_v) conversion terms that represent the covariances of potential temperature and horizontal and vertical flow fluctuations in the direction of the ensemble mean potential temperature gradient; (3) the term C represents a diabatic generation (source/sink) term resulting from the covariance of fluctuations of potential temperature and diabatic heating rate (J_n'), including contributions from radiation heating (C_{rad}), latent heat release (C_{cond}), convective heating (C_{conv}), and boundary layer heating, namely turbulent vertical diffusion (C_{dv}) and lateral diffusion (C_{dh}); and (4) the third-order term (E) is the covariance of the potential temperature fluctuations and divergence of potential temperature flux due to fluctuations.

[17] In this study we will use absolute vorticity rather than relative vorticity as in NL10. The IV budget equation for absolute vorticity can be established similarly to that of relative vorticity and it is written as:

$$L_\eta = R_\eta = A_h + A_v + N + B_h + B_v + C + E + F + G + H \quad (8)$$

where the terms are given by:

$$L_\eta = \frac{\partial \sigma_\eta^2}{\partial t};$$

$$A_h = -\vec{\nabla} \bullet \langle \sigma_\eta^2 \langle \vec{V} \rangle \rangle; \quad A_v = -\frac{\partial \langle \sigma_\theta^2 \langle \omega \rangle \rangle}{\partial p};$$

$$B_h = -2 \langle \eta_n' \vec{V}_n' \rangle \bullet \vec{\nabla} \langle \eta \rangle; \quad B_v = -2 \langle \eta_n' \omega_n' \rangle \frac{\partial \langle \eta \rangle}{\partial p}$$

$$C = -2 \langle \eta \rangle \langle \eta_n' \vec{\nabla} \bullet \vec{V}_n' \rangle; \quad N = -2 \sigma_n^2 \vec{\nabla} \bullet \langle \vec{V} \rangle$$

$$E = 2S \left[\frac{\partial \langle \omega \rangle}{\partial Y} \langle \eta_n' \frac{\partial U_n'}{\partial p} \rangle - \frac{\partial \langle \omega \rangle}{\partial X} \langle \eta_n' \frac{\partial V_n'}{\partial p} \rangle \right];$$

$$F = 2S \left[\langle \eta_n' \frac{\partial \omega_n'}{\partial Y} \rangle \frac{\partial \langle U \rangle}{\partial p} - \langle \eta_n' \frac{\partial \omega_n'}{\partial X} \rangle \frac{\partial \langle V \rangle}{\partial p} \right];$$

$$G = 2S \left[\langle \eta_n' \frac{\partial F_{Yn}'}{\partial X} \rangle - \langle \eta_n' \frac{\partial F_{Xn}'}{\partial Y} \rangle \right] - 2c \langle \eta_n' \nabla^4 \eta_n' \rangle;$$

$$H = -2 \langle \eta_n' \vec{\nabla} \bullet \langle \eta_n' \vec{V}_n' \rangle \rangle - \langle \omega_n' \frac{\partial \eta_n'^2}{\partial p} \rangle$$

$$+ 2S \left[\langle \eta_n' \frac{\partial \omega_n'}{\partial Y} \frac{\partial U_n'}{\partial p} \rangle - \langle \eta_n' \frac{\partial \omega_n'}{\partial X} \frac{\partial V_n'}{\partial p} \rangle \right]$$

where $S \equiv m^2 = (1 + \sin \psi_0)/(1 + \sin \psi)$ is the metric term for a polar stereographic projection; ψ and ψ_0 are the local and reference latitudes, respectively; $c = 1.85 \times 10^{13} \text{ m}^4 \text{ s}^{-1}$ is a constant used in the CRCM to compute the lateral diffusion

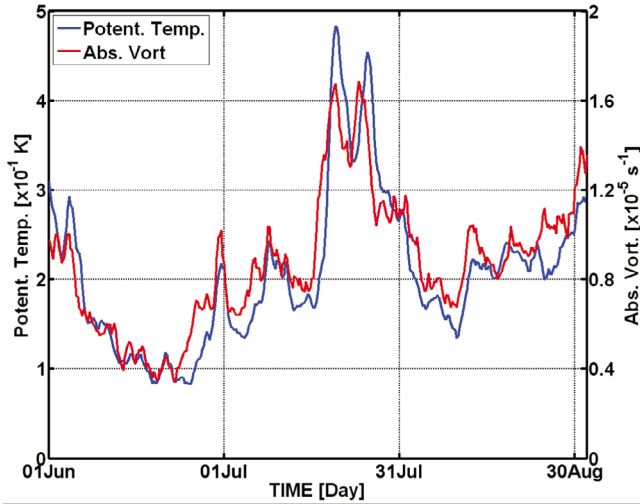


Figure 1. Time evolution of the vertical and domain average of the internal variability standard deviation for the potential temperature (blue) and the absolute vorticity (red).

[Laprise et al., 1998]. The term L_η represents the local rate of change of absolute vorticity IV, and R_η is the sum of eight terms that contribute to the tendency. As before, terms A relate to the IV transport by the ensemble mean flow and terms B relate to the covariance of fluctuations (η'_n and \vec{V}'_n) in the direction of the gradient of the ensemble mean absolute vorticity ($\nabla \langle \eta \rangle$). The term N is the divergence of the ensemble mean horizontal wind acting upon IV. The term C couples the ensemble mean absolute vorticity $\langle \eta \rangle$ and the covariance of perturbations of absolute vorticity and horizontal divergence $\langle \eta'_n \nabla \cdot \vec{V}'_n \rangle$. Terms E and F arise from the tilting-twisting term in the vorticity equation. The term E combines the horizontal gradient of the ensemble mean vertical motion to the covariance of fluctuations of the absolute vorticity and the vertical shear of the horizontal flow. The term F combines the vertical shear of the ensemble mean horizontal flow to the covariance of fluctuations of the absolute vorticity and the horizontal gradient of the vertical motion. The term G is the sum of covariance terms involving absolute vorticity and horizontal stress perturbations: the first two terms are a coupling with the horizontal gradient of vertical diffusion and sources/sinks of momentum, and the third is associated with the lateral diffusion. The last term (H) regroups third-order terms.

[18] The absolute vorticity IV equation is similar to relative vorticity IV equation used by NL10, except for the term D in the latter that accounted for the Coriolis parameter.

[19] The differential terms in these equations were evaluated by using standard discretization methods, as per NL10.

3. Results and Analysis

[20] This section will focus on the description and physical interpretation of different terms in IV budget equations at the seasonal scale. First, we will analyze and compare the seasonal IV and TV over the whole troposphere for the 1993 summer season. Then, we will discuss the summer ‘climatology’ of various contributions to the IV tendency. To

identify dominant terms, we will first examine the domain-averaged vertical profile and time evolution of these contributions. All maps are shown excluding the 10-grid point sponge zone around the border of the model domain.

3.1. 1993 Summer Climatology of the IV

[21] Figure 1 presents the time evolutions of the vertically averaged and domain-averaged potential temperature and absolute vorticity IV. During the 1993 summer, results indicate that the IV (expressed in terms of standard deviations) fluctuates between 0.1 and 0.5 K for potential temperature and between $0.4 \cdot 10^{-5}$ and $2 \cdot 10^{-5} \text{ s}^{-1}$ for absolute vorticity. For both variables, the IV fluctuates greatly in time, with occasional episodes of intense IV at certain times, such as those in the last 15 days of July 1993. Results also show a very strong relationship between the time evolutions of IV for the two studied variables, with a correlation coefficient about 0.92; this result confirms previous studies indicating that the IV is tied to synoptic events [e.g., Giorgi and Bi, 2000; Alexandru et al. 2007; NL10].

[22] Figures 2a, 2b, 3a, and 3b show the horizontal distributions of the vertical average over the troposphere (equation (6)) of the time-averaged IV $\left(\sqrt{\langle \sigma_\varphi^2 \rangle^p} \right)$ and the ensemble mean TE $\left(\sqrt{\langle \sigma_\varphi^2 \rangle^p} \right)$ for potential temperature (Figures 2a and 3a) and absolute vorticity, respectively, for the 1993 summer season simulations. The horizontal distributions of IV for the two studied variables share a number of common features. Due to the imposed LBC, IV vanishes at the border of the model domain (not shown in the maps). There is a maximum potential temperature IV located over the northeast part of the study domain, on the downstream side of the dominant southwesterly flow. The absolute vorticity IV exhibits an elongated maximum extending to southwestward of the domain, along the East Coast of the United States. This distribution of the IV seems to corroborate the interpretation that the most intense IV occurs along the storm track [Alexandru et al., 2007]. They noted that the IV center is initially formed over the southern U.S., intensifies and moves northeastward along the storm track in the following days.

[23] Figures 2b and 3b show the horizontal distributions of the vertically averaged ensemble mean TV for the two studied variables. The maximum potential temperature TV is located over the northwest part of the study domain (Figure 3b). In term of magnitude, we note that the TV values are 10 times stronger than the IV (note the different scales for IV and TV standard deviations in Figures 2 and 3). The standard deviation of IV is a few tenths of degree for potential temperature (Figure 2a) and of order of 10^{-5} s^{-1} for absolute vorticity (Figure 3a), whereas the TV standard deviation reaches values of 5 K and $8 \cdot 10^{-5} \text{ s}^{-1}$ for the potential temperature (Figure 2b) and the absolute vorticity (Figure 3b), respectively. We note a small area of maximum absolute vorticity IV and TV over Alabama, which appears to be associated with intense convection there and is also reflected in a maximum of potential temperature IV there.

[24] Figures 2c, 2d, 3c, and 3d show the vertical profiles of standard deviations of the domain-averaged IV and TV for the potential temperature and the absolute vorticity,

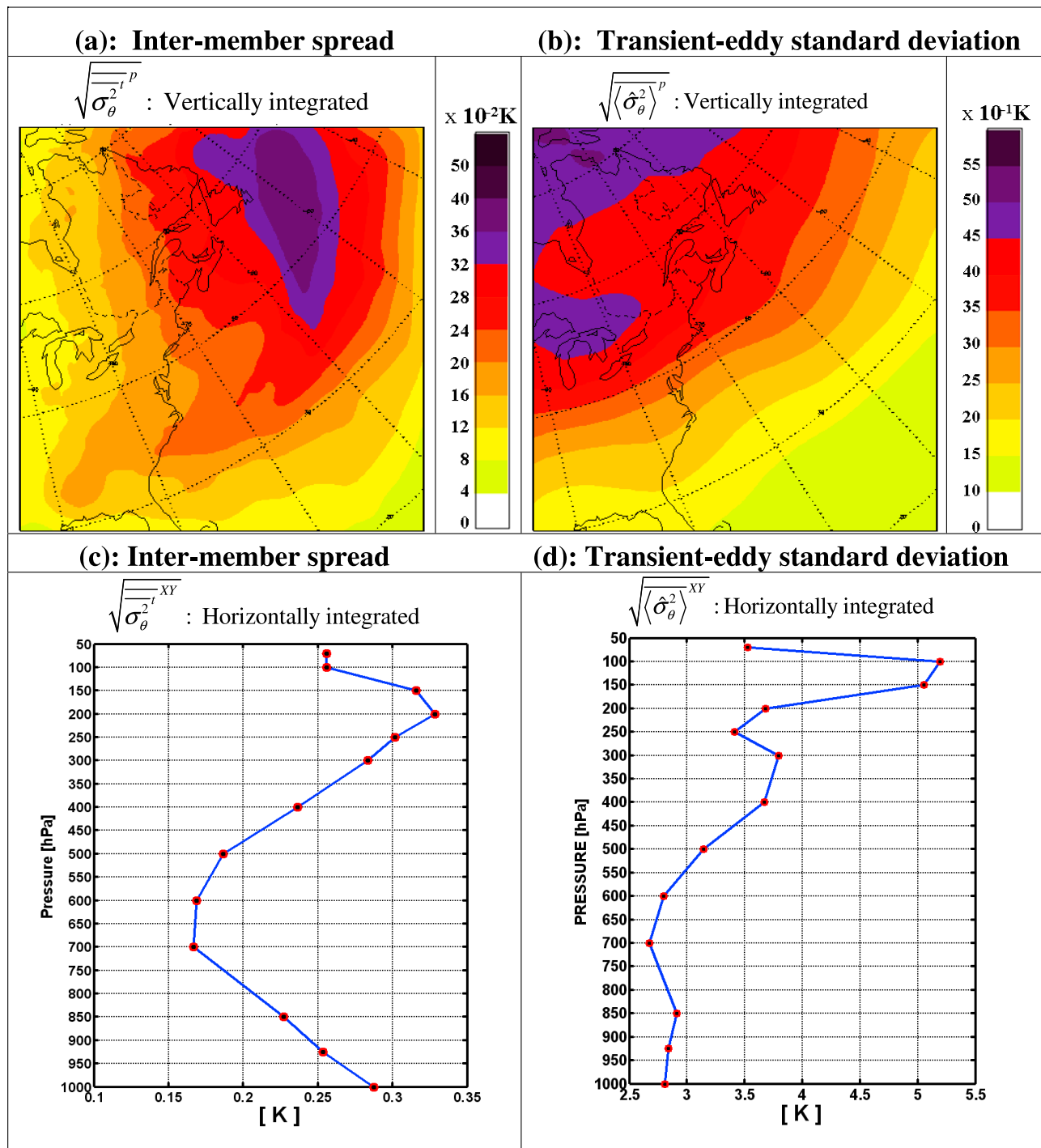


Figure 2. For potential temperature: (a) square root of the time average and vertical integral of the internal variability variance and (b) square root of the vertical integral of the ensemble mean transient-eddy variance. (c) Square root of the vertical profile of the internal variability variance, and (d) square root of the ensemble mean transient-eddy variance. Note the different scales for internal variability and transient-eddy standard deviations.

respectively. These profiles are roughly similar, with a maximum near the surface, a minimum in mid troposphere, and another maximum near the tropopause. The potential temperature standard deviation IV varies from 0.28 K near the ground to a minimum of 0.16 K at around 600–700 hPa, and reaches a maximum value of about 0.33 K at 200 hPa

(Figure 2c). A similar profile is noted for the absolute vorticity with a maximum of $1.3 \cdot 10^{-5} \text{ s}^{-1}$ near the ground, a minimum of $0.7 \cdot 10^{-5} \text{ s}^{-1}$ at around 600–700 hPa and another maximum of $1.1 \cdot 10^{-5} \text{ s}^{-1}$ at 300 hPa (see Figure 3c). Compared to IV, the TE standard deviation has similar vertical profile and large magnitude, around 10 times greater

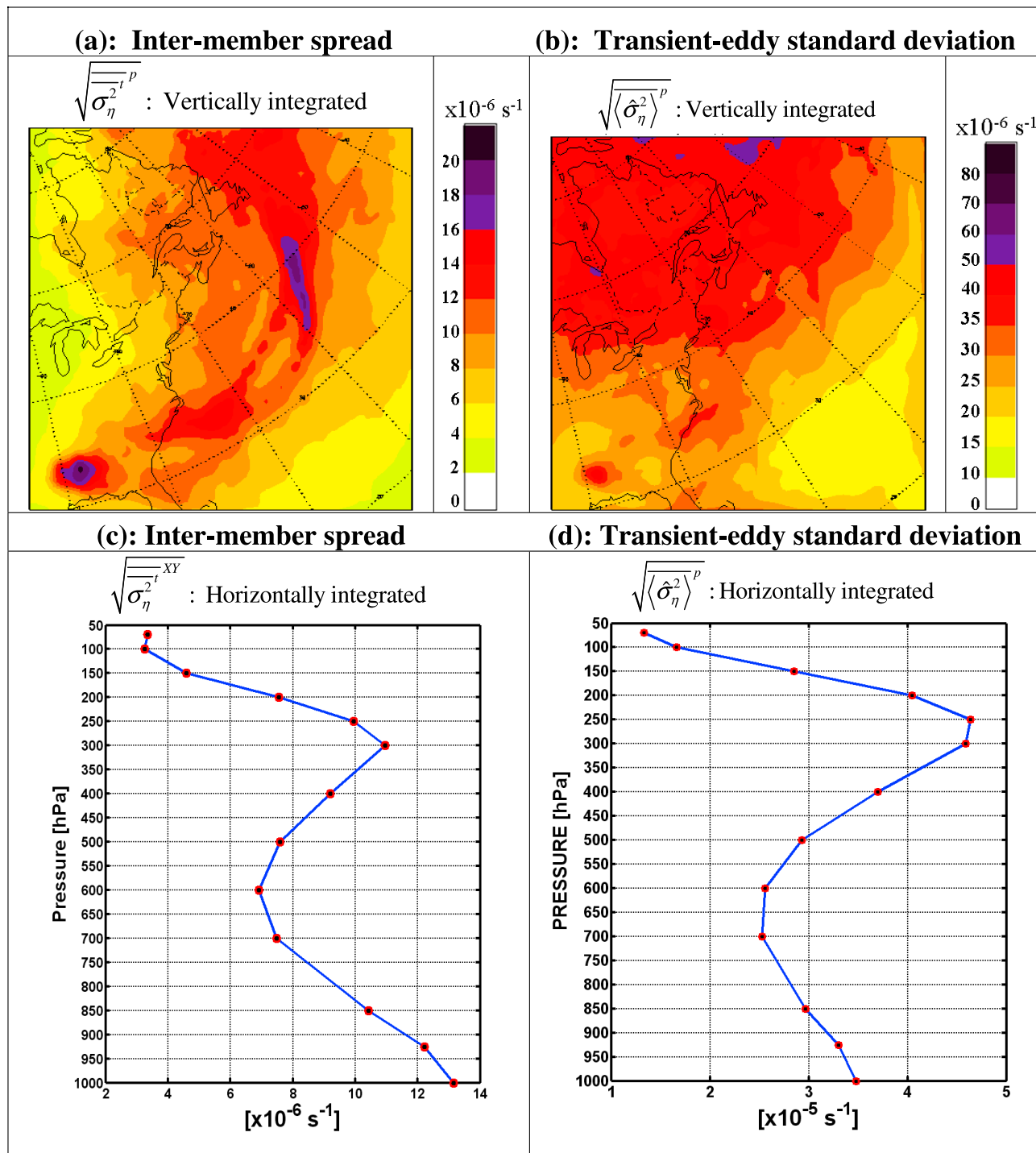


Figure 3. For absolute vorticity: (a) square root of the time average and vertical integral of the internal variability variance and (b) square root of the vertical integral of the ensemble mean transient-eddy variance. (c) Square root of the vertical profile of the internal variability variance, and (d) square root of the ensemble mean transient-eddy variance. Note the different scales for internal variability and transient-eddy standard deviations.

than the IV (Figure 2c versus Figure 2d and Figure 3c versus Figure 3d). On average, the potential temperature TE standard deviation slightly fluctuates from 2.8 K at 1000 hPa to 3.4 K at 250 hPa, with a minimum value of 2.6 K in the midtroposphere (Figure 2d). For absolute vorticity, we note

a large variation between the middle and top and bottom of the troposphere as it was noted for IV: $3.5 \times 10^{-5} \text{ s}^{-1}$ at 1000 hPa, $2.6 \times 10^{-5} \text{ s}^{-1}$ at 600–700 hPa, and $4.7 \times 10^{-5} \text{ s}^{-1}$ at 250 hPa (see Figures 3c and 3d).

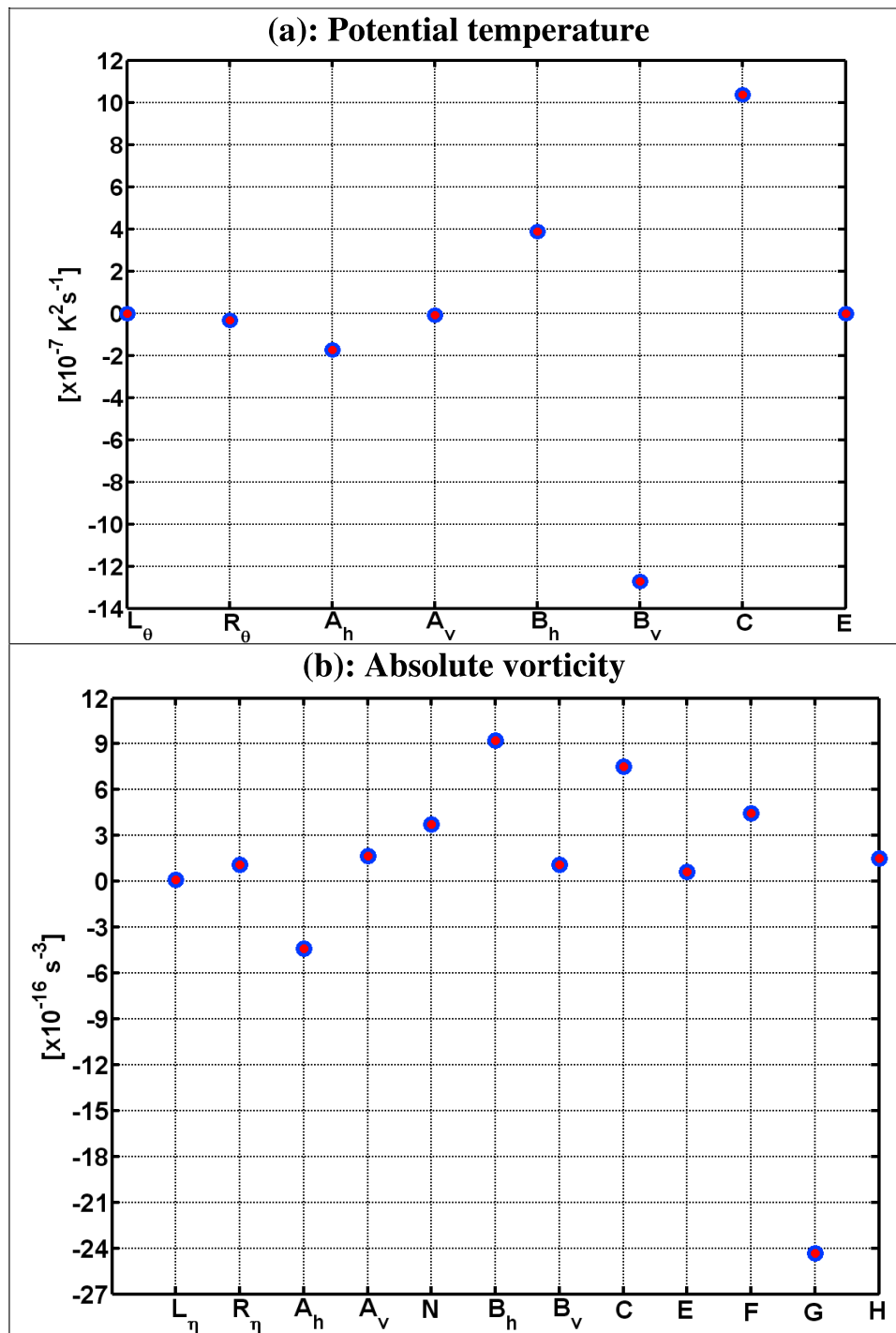


Figure 4. Domain average of the vertical integral over the troposphere (250 to 1000 hPa) of the time average of different terms in the IV budget equation for (a) the potential temperature and (b) the absolute vorticity.

3.2. Time- and Domain-Averaged IV Budget

[25] In this section, we present the 1993 summer “climatology” of the contributions of the different terms to the time mean and domain-averaged IV budget. Starting with the IV equations (equations (7) and (8)), time averaging was applied (equation (4)), followed by horizontal averaging (equation (5)) and vertical averaging (equation (6)), thus

reducing the dimensionality of the budget to a strict minimum. Figure 4 shows the resulting values of each term of the IV budget equations for potential temperature and absolute vorticity. We note that the time average of the tendency terms (L_θ and L_η) are nearly zero, indicating that there is no net trend in IV in the simulations, despite the fact that the IV strongly fluctuates with synoptic events during the simulations. The sums of all right-hand terms (terms R)

are also close to zero; the near equality between the IV tendency term and the sum of all terms on the right-hand side comforts us that we are able to adequately compute diagnostically the major contributions occurring during the simulations, despite time sampling and several interpolations and discretization approximations, as discussed by NL10.

[26] Figure 4a shows that the dominant terms for the potential temperature IV are B_v , C , B_h and A_h , with on average B_h and C contributing to the growth of IV, whereas A_h and B_v are negative contributions. The largest positive contribution is the covariance of fluctuations of potential temperature and diabatic heating rate (term C), whereas the largest negative contribution is the covariance fluctuations of potential temperature and vertical velocity acting upon the ensemble mean potential temperature gradient (term B_v). The term B_h is the second positive contribution, while the horizontal transport term (A_h) acts as a secondary negative contribution. The other terms, the vertical transport of the potential temperature IV (term A_v) and the third-order terms (term E), are negligible. At the seasonal scale, it appears from Figure 4a that, on average, the sum ($B_h + C$) is in approximate balance with the sum of A_h and B_v .

[27] For the budget equation of the absolute vorticity IV, Figure 4b indicates that six terms are dominant on the right-hand side of the equation (G , B_h , C , A_h , N and F) and the remaining four terms contribute very little to the seasonal tendency (A_v , B_v , E and H). Of the dominant terms, two (G and A_h) are negative contributions and four (B_h , C , N and F) are positive contributions to the tendency, so there exists an approximate balance between ($G + A_h$) and ($B_h + C + N + F$).

3.3. Vertical Profile of Contributions to IV Budget

[28] Having identified the respective contributions from the various terms to the domain-averaged IV budget, we now turn our attention to the vertical structure of the contributing terms.

[29] Figure 5 shows the vertical profiles of the time mean and horizontal average of each term in the IV budget equations for the potential temperature (Figure 5a) and the absolute vorticity (Figure 5b). For each variable, graphs are represented in two panels in order to separate terms according to their order of magnitude: Figures 5a (left) and 5b (left) display the dominant terms, while the weaker contributions are shown in Figures 5a (right) and 5b (right) (note the different scales). It is clearly seen that tendency terms (L) are nearly zero at all pressure levels for both variables (blue lines in Figures 5a (right) and 5b (right)). For the two studied variables, the sum of all terms on the right-hand side (term R) is not perfectly zero owing to numerical approximations made in calculating the contributions, but it has weak amplitude at all levels (red lines in Figures 5a (right) and 5b (right)). The largest errors occur near the tropopause level for potential temperature where simulated variables exhibit rapid variations, resulting in larger numerical errors when computing gradients with finite differences and few pressure levels.

[30] For the potential temperature IV, Figure 5a (left) shows the vertical profile of the four dominant terms: A_h , B_h , B_v and C . Between 925 hPa and 250 hPa, B_h and C represent positive contributions to the summer IV tendency, while A_h and B_v act in opposite way as negative contributions, which

confirms that the compensation occurring in the vertically integrated IV statistics, as noted section 3.2, also occurs at each level in this part of the troposphere. Near the surface, term C turns into a negative contribution because contributions of horizontal and vertical diffusions dominate positive contributions. Around 1000 hPa, B_h becomes very large whereas B_v is zero. Results show that the positive large value of B_h is associated with a large covariance of potential temperature and horizontal flow fluctuations (result not shown), as a result of important fluctuations near the ground. The contribution of B_v to IV is weak at 1000 hPa because the vertical motion is zero on the ground. Contrary to what is observed in the middle troposphere, Figure 5 shows a change in the behaviors of B_v and C in the upper troposphere. The positive sign of B_v and the negative sign of C in this region are associated with a positive covariance of fluctuations ($\langle \theta'_n \omega'_n \rangle > 0$) and a dominant negative contribution of diffusion processes, respectively.

[31] In terms of large contributions, the most dominant terms are B_v and C that counteract each other above the 925 hPa level; the maximum contributions of these two terms are located at 400 and 850 hPa, with a magnitude of about $2 \times 10^{-6} K^2 s^{-1}$. To get a physical sense of the meaning of these numbers, we note that a contribution of $10^{-6} K^2 s^{-1}$ represents a variation of about $(0.3K)^2$ per day to the potential temperature variance. The terms A_v and E (Figure 5a, right) are smaller than the other terms at all pressure levels.

[32] Figure 5b shows the vertical profile of the terms in the absolute vorticity IV budget equation. Figure 5b (left) shows the vertical profile of dominant terms: A_h , B_h , C , F , N and G . It can be noted that two terms (A_h and G) have negative values at all pressure levels and four terms (B_h , C , F and N) have positive values. Thus the vanishing time-averaged tendency results from an approximate balance between ($B_h + C + F + N$) and ($A_h + G$). The terms C and G have the largest positive and negative contributions near the ground, with values of about $7 \times 10^{-15} s^{-3}$ and $-12 \times 10^{-15} s^{-3}$, respectively. Physically a contribution of the order of $10 \times 10^{-15} s^{-3}$ corresponds to a change of the absolute vorticity variance of approximately $(0.3 \times 10^{-4} s^{-1})^2$ per day. Except for the term F that acts in the upper half of the troposphere, the largest contributions to the absolute vorticity IV budget occur near the ground and at the vicinity of the tropopause (around 300 hPa). Contrary to the potential temperature, the important terms for the absolute vorticity act mostly in these two regions of the atmosphere. In addition to terms L_η and R_η , the weak contribution terms are plotted in Figure 5b (right), namely A_v , B_v , E and H . On average, their amplitude is less than $0.8 \times 10^{-15} s^{-3}$ at all pressure levels, whereas the larger contributions (Figure 5b, left) exceed $5 \times 10^{-15} s^{-3}$.

3.4. Time Evolution of the Vertical and Domain Average of Contributions to IV Budget

[33] Figures 6 and 7 present the time evolution of the vertical and domain average of various contributions to IV tendencies and a comparison of the left- and right-hand side terms, for potential temperature and absolute vorticity respectively. In Figures 6a and 7a, different colors represent the contribution of each term in IV budget equations. The results show that individual terms tend to act systematically

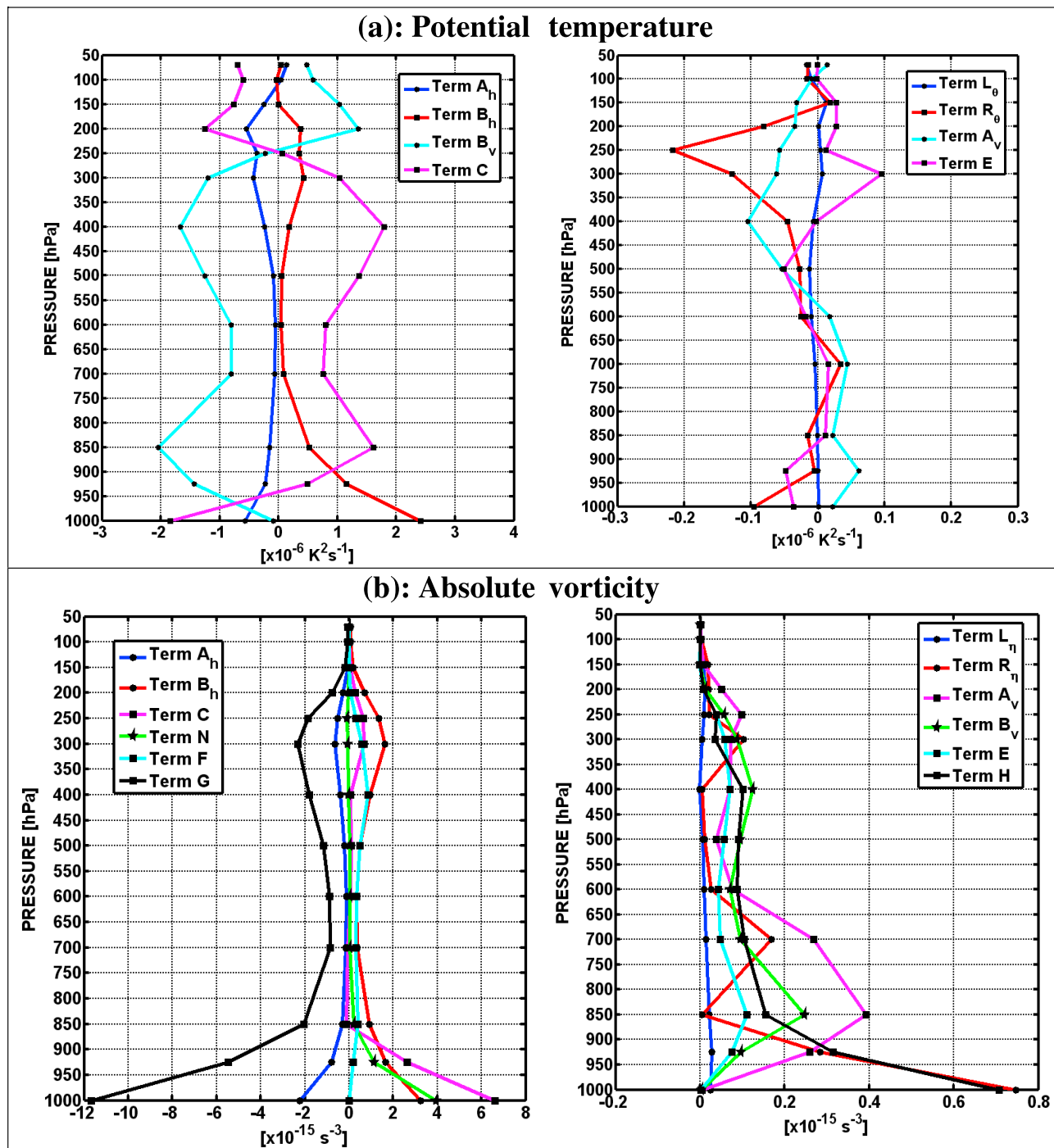


Figure 5. Vertical profiles of the time and domain average of different terms in the interspread variance equation for (a) potential temperature and (b) absolute vorticity.

as either a positive or a negative contribution to the IV tendency. The time fluctuation of positive and negative contributions seem to follow closely one another, as it can be noted between the middle and the end of July. As can be seen in Figures 6b and 7b showing the left-hand side term $(L_\varphi(t)^{pXY})$ and the sum of all right-hand side terms $(R_\varphi(t)^{pXY})$, the time fluctuation of IV in fact result from the imperfect cancellation of the positive and negative contribution to the IV tendency. Note that the individual con-

tributions to the IV tendency are more than one order of magnitude larger than the resulting IV. For the potential temperature, it is clearly seen in Figure 6a that B_h and C are positive contributions while the others terms (B_v , A_h , A_v and E) are negative during the three months of 1993 summer. The dominant positive and negative contributions to the IV tendency are C and B_v and the weaker contributions are A_v and E . Figure 7a shows different contributions to the absolute vorticity IV tendency. We note that terms A_h and G

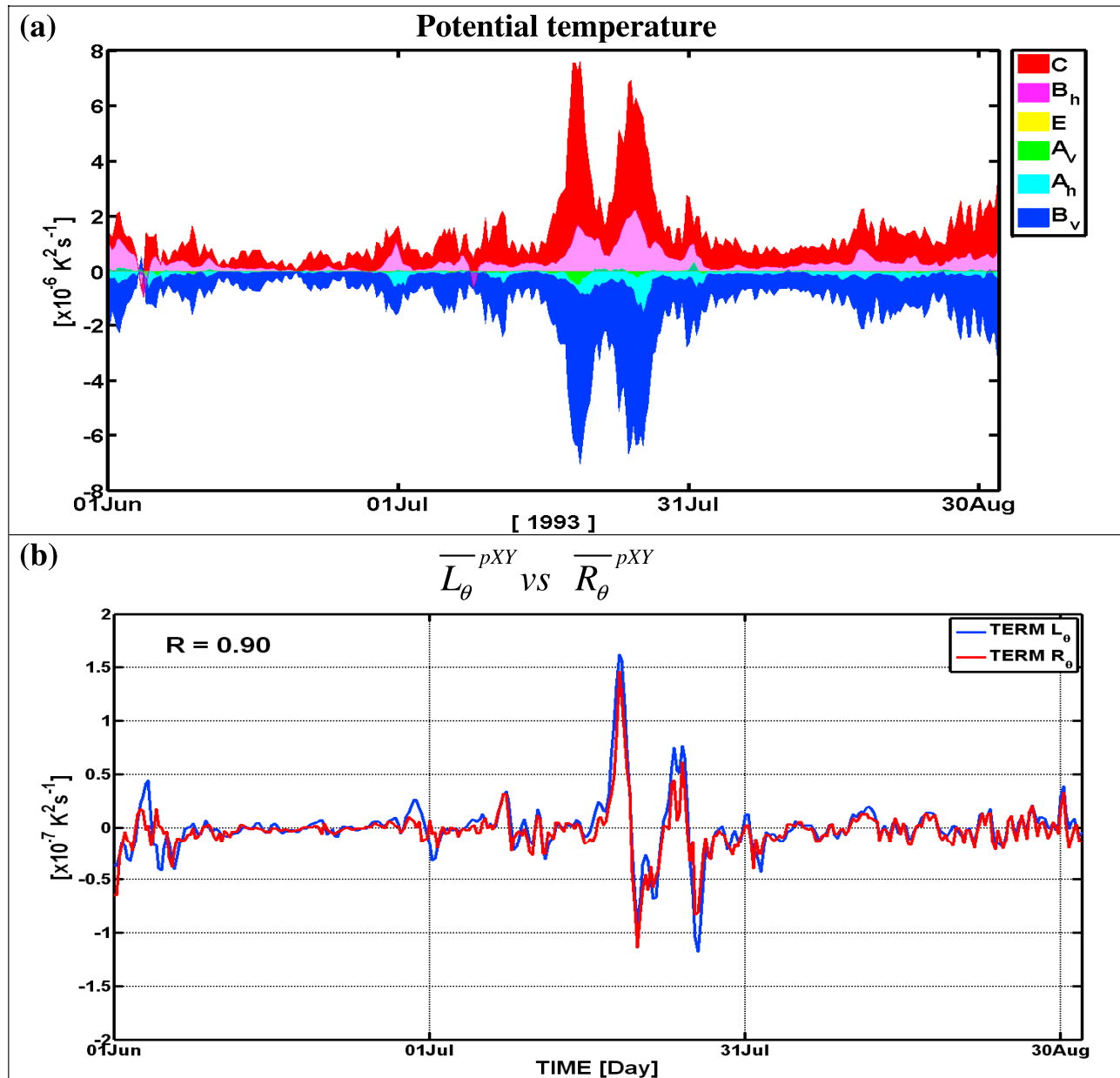


Figure 6. The time evolution of domain average and vertical integration over the whole troposphere of different terms in the IV budget equation of the potential temperature.

act in the opposite way to the others terms (B_h , C , F , N , A_v , H , B_v and E). Although, we note weak positive contributions of A_v , H , B_v and E during the three months, result reveal that the third-order term (H) becomes large when the IV is particularly intense (see green color in the last 15 days of July in Figure 7a).

[34] Figures 6b and 7b present the comparison between the left- and right-hand side terms averaged over the vertical and horizontal domain for the potential temperature and the absolute vorticity, respectively. These results denote fairly good agreement, with correlations coefficient of 0.90 for potential temperature and 0.95 for absolute vorticity. This result indicates good agreement between the IV tendency developed in the CRCM simulations and the sum of various complex terms of the diagnostic calculation.

3.5. Horizontal Distribution of Contributions to IV Budget

[35] The dimension reduction afforded by domain averaging of the IV budget equations gave an overall view of various contributions to the IV budget. We found that depending on the studied variable, certain terms contribute only weakly. These results show that the IV budget for the 1993 summer is due to an approximate balance between four terms for potential temperature and six terms for absolute vorticity. In this section, we analyze the spatial pattern of the significant terms, under vertical integration to reduce the dimensionality of fields.

[36] Figure 8 shows the spatial pattern of the time-averaged and vertically averaged contributions in the tropo-

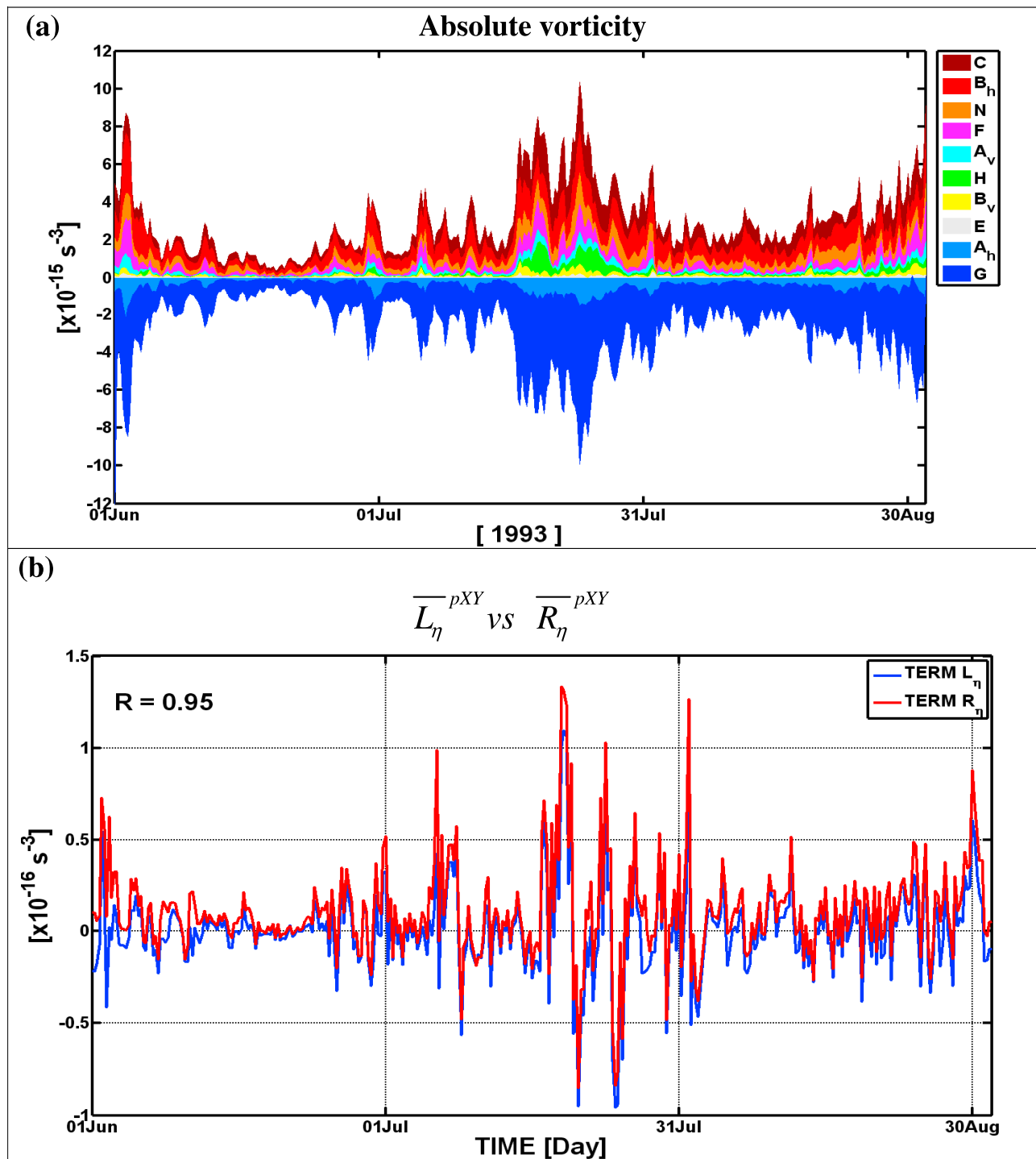


Figure 7. The time evolution of domain average and vertical integral over the whole troposphere of different terms in the IV budget equation of the absolute vorticity.

sphere of the dominant terms (A_h , B_h , B_v and C) for the IV budget equation of potential temperature. As shown in the previous results (Figure 5), it is clearly seen that B_h and C are mainly positive fields, so they act to generate IV during this season. The term C exhibits the largest and the most intense positive contribution to the time-averaged IV tendency. High intensities are located over a small area over the

southern U.S. (Alabama) and along the storm track in the Atlantic Ocean. The analysis of various contributions to the term C (Figure 9) indicates that the intense positive contributions are mainly due to effects of two physical processes: condensation (C_{cond}) and convection (C_{conv}) (Figures 9b and 9c). The pattern associated to the radiation process (C_{rad}) is also positive over a large area, but less

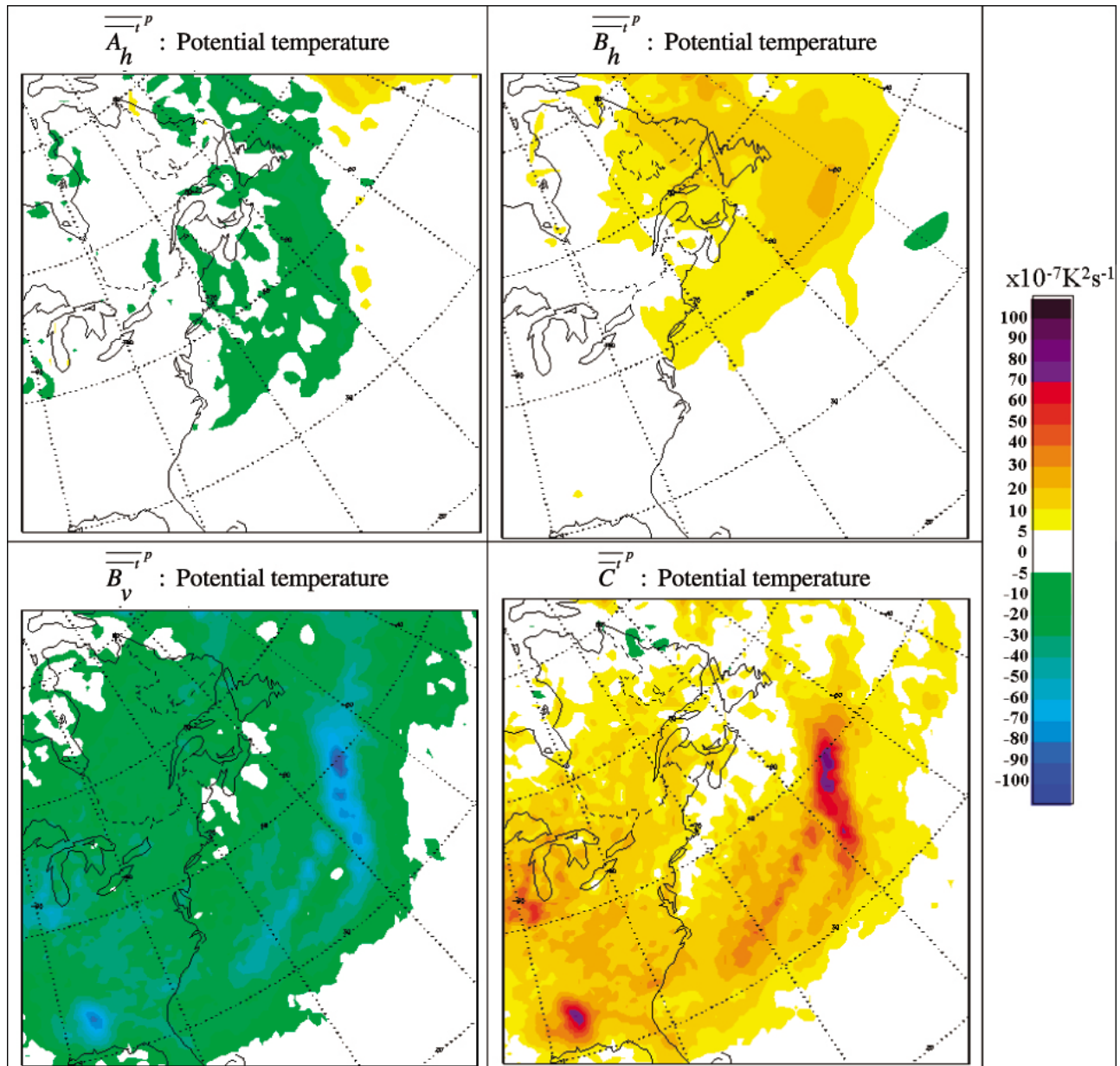


Figure 8. Vertical integral over the whole troposphere of the time average of different terms in the intermember variance equation for the potential temperature.

intense (Figure 9d). On the other hand, the horizontal and vertical diffusions (C_{dv} and C_{dh}) act to reduce the large positive contributions from the other terms of C , with mostly negative contributions (Figures 9e and 9f). The term B_h is also a positive contribution of the seasonal IV, particularly over the northeastern part of the study domain (Figure 8, top right). The analysis of the different components of B_h sheds light on the physical meaning of its positive contribution to the time-averaged IV tendency. As shown in Figure 10a, the time average and vertical average of the covariance $\overline{\langle U'_n \theta'_n \rangle}^p$ in the troposphere is negative in this region, while the time average of eastward gradient of the ensemble mean potential temperature is positive ($\overline{\langle \partial \langle \theta \rangle / \partial X^p} > 0$), result not

shown). This means that, on average in the whole troposphere, the transport of warm perturbations ($\theta'_n > 0$) by westward wind perturbations ($U'_n < 0$), hence down the ensemble mean gradient of potential temperature, favors the growth of IV during this season. For the north–south contribution in B_h , the results indicate that the time-averaged and vertically averaged covariance of fluctuations $\overline{\langle V'_n \theta'_n \rangle}^p$ has a positive sign (see Figure 10b), while the northward gradient of ensemble mean potential temperature is negative ($\overline{\langle \partial \langle \theta \rangle / \partial Y^p} < 0$, not shown). Therefore, the positive contribution to IV tendency arises from a transport of warm perturbation ($\theta'_n > 0$) northward ($V'_n > 0$), again down the ensemble mean gradient of potential temperature.

Potential temperature: $\overline{C}^p = \overline{C_{cond}^p} + \overline{C_{conv}^p} + \overline{C_{rad}^p} + \overline{C_{dv}^p} + \overline{C_{dh}^p}$

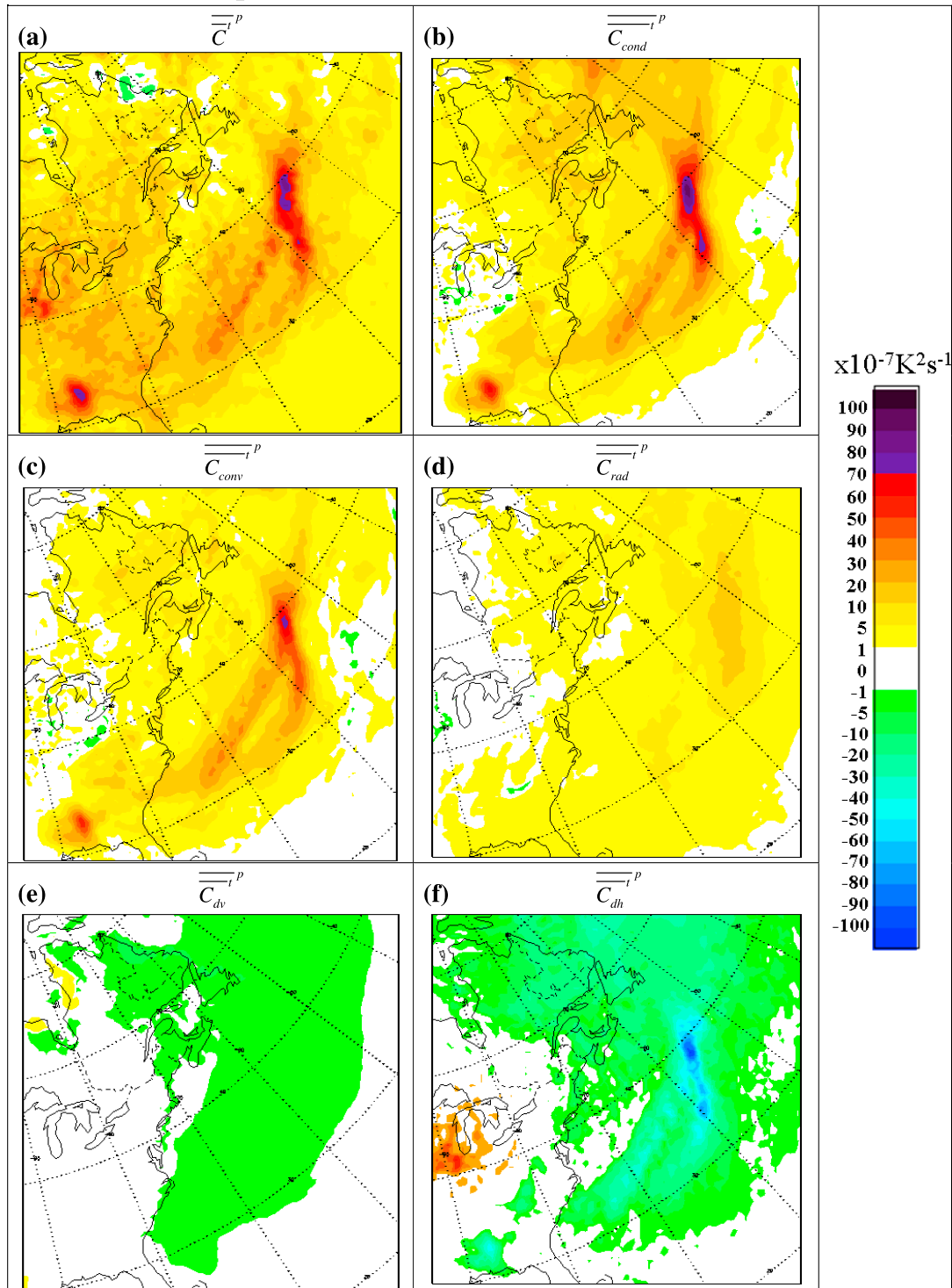


Figure 9. Vertical integral over the whole troposphere of the time average of different contributions to the term C (a) in the intermember variance equation for the potential temperature. Contributions: (b) condensation, (c) convection, (d) radiation, (e) vertical diffusion and (f) horizontal diffusion.

[37] The potential temperature IV tends to be reduced by the negative contribution from B_v (Figure 8, bottom left). In fact Figure 8 shows that B_v and C exhibit similar patterns, but of opposite signs. This result confirms the preceding

findings that indicated that B_v and C contribute in opposite ways to the IV tendency. In fact, the negative sign of the time average of B_v in the troposphere is associated with a

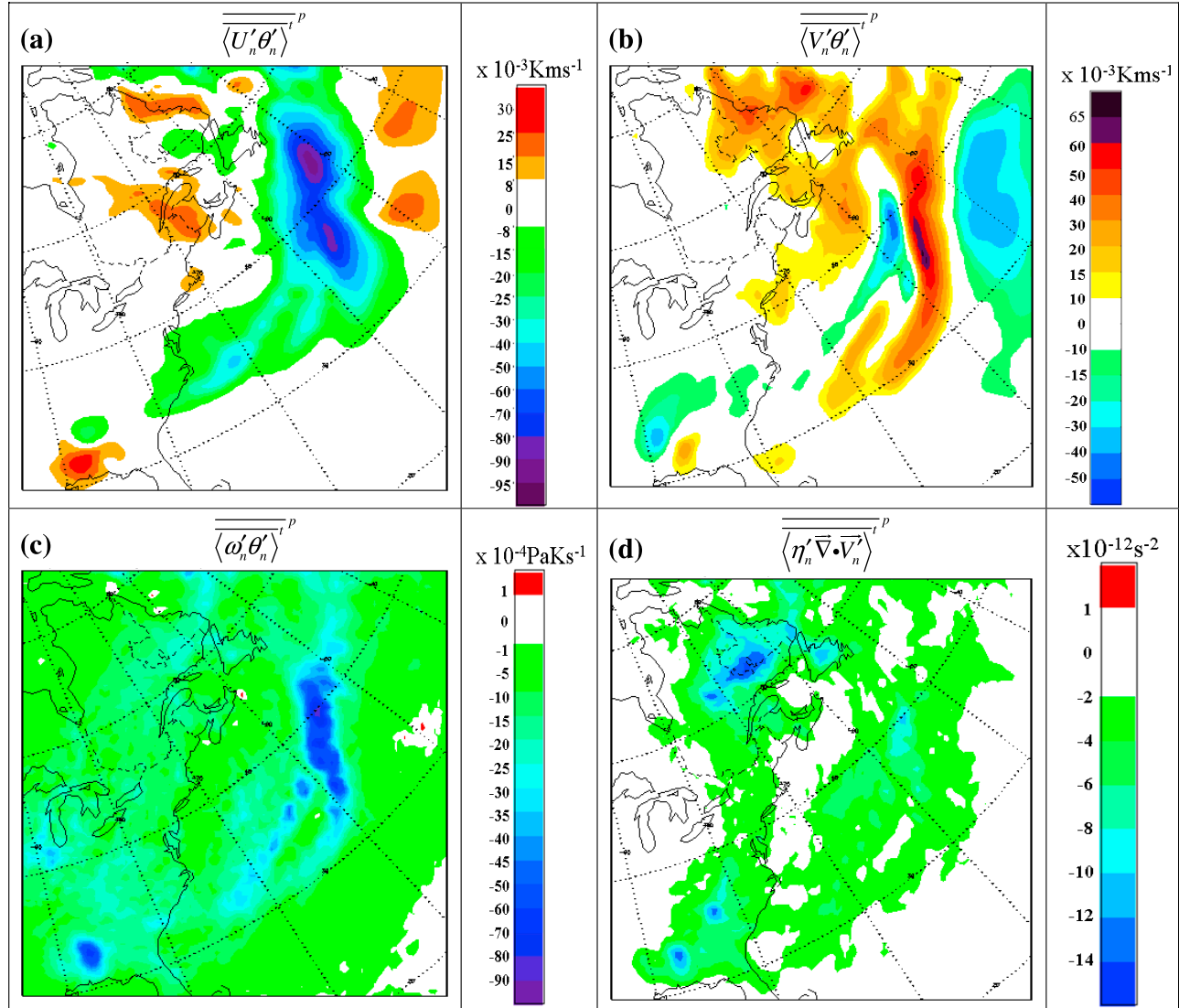


Figure 10. Vertical integral of the time average of the covariance of fluctuations in (a and b) B_h and (c) B_v of the potential temperature IV, and (d) the covariance of fluctuations in C of the absolute vorticity.

negative covariance of fluctuation ($\overline{\langle \theta'_n \omega'_n \rangle}^p < 0$); see Figure 10c) in a stable environment (i.e., $\partial \langle \theta \rangle / \partial p < 0$) of the ensemble mean atmosphere. Physically, this means that warm air rises and cold air sinks in perturbations from the ensemble mean conditions. Thus, static stability tends to suppress, or consume, the potential temperature IV. The horizontal transport term (A_h) of the IV equation also acts as a sink term (Figure 8, top left), which makes sense since the IV transport out of the study domain by the ensemble mean flow tends to reduce the IV.

[38] We will now proceed to the analysis of the dominant terms in the absolute vorticity IV budget: A_h , B_h , C , F , N and G . Figure 11 presents the time average and vertical averaging in the troposphere of these dominant terms for the 1993 summer simulations. The positive contributions to the seasonal IV budget are B_h , C , N and F , and negative contributions are G and A_h . Similarly to the potential temperature, B_h acts as a production term for the IV because the

covariance vector ($\overline{\langle \eta'_n \nabla \cdot \mathbf{V}'_n \rangle}^p$) is in the opposite direction to the horizontal gradient of the ensemble mean absolute vorticity ($\nabla \langle \eta \rangle$), indicating transport of perturbation vorticity is down the gradient of the ensemble mean absolute vorticity. The term C is the second largest positive contribution to the absolute vorticity IV budget, due to a negative distribution of the covariance perturbations of absolute vorticity and horizontal divergence $\overline{\langle \eta'_n \nabla \cdot \mathbf{V}'_n \rangle}^p < 0$ (Figure 10d).

Therefore, the positive/negative perturbations of the absolute vorticity are associated with the convergence/divergence of the horizontal flow perturbations. Similarly, results indicate that the positive contribution of N is associated with the convergence of the ensemble mean motion. Finally, the term F is a weak positive contribution to the time-averaged IV tendency; this result is due to the positive contribution of the

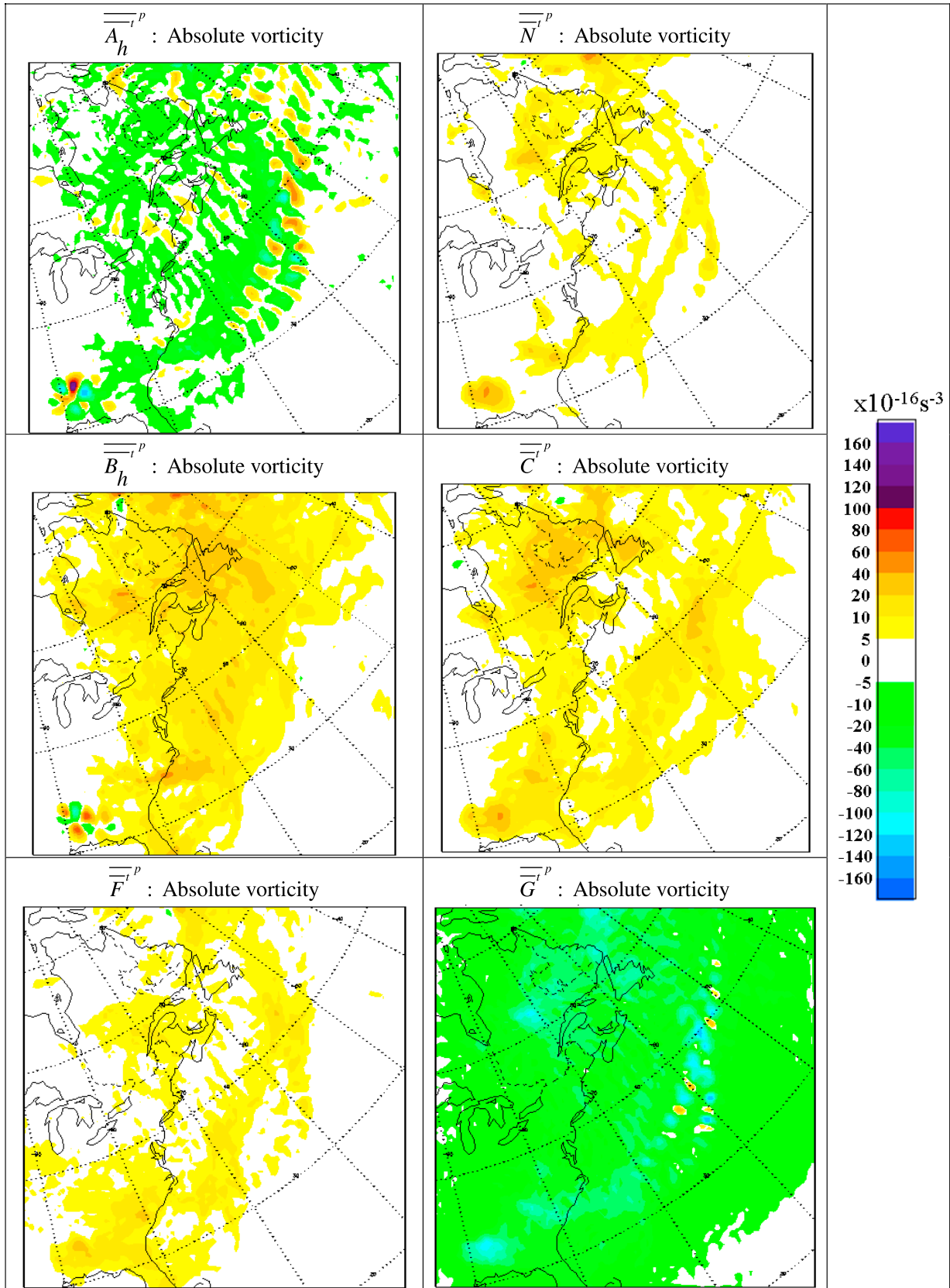


Figure 11. Vertical integral over the whole troposphere of the time average of different terms in the intermember variance equation for the absolute vorticity.

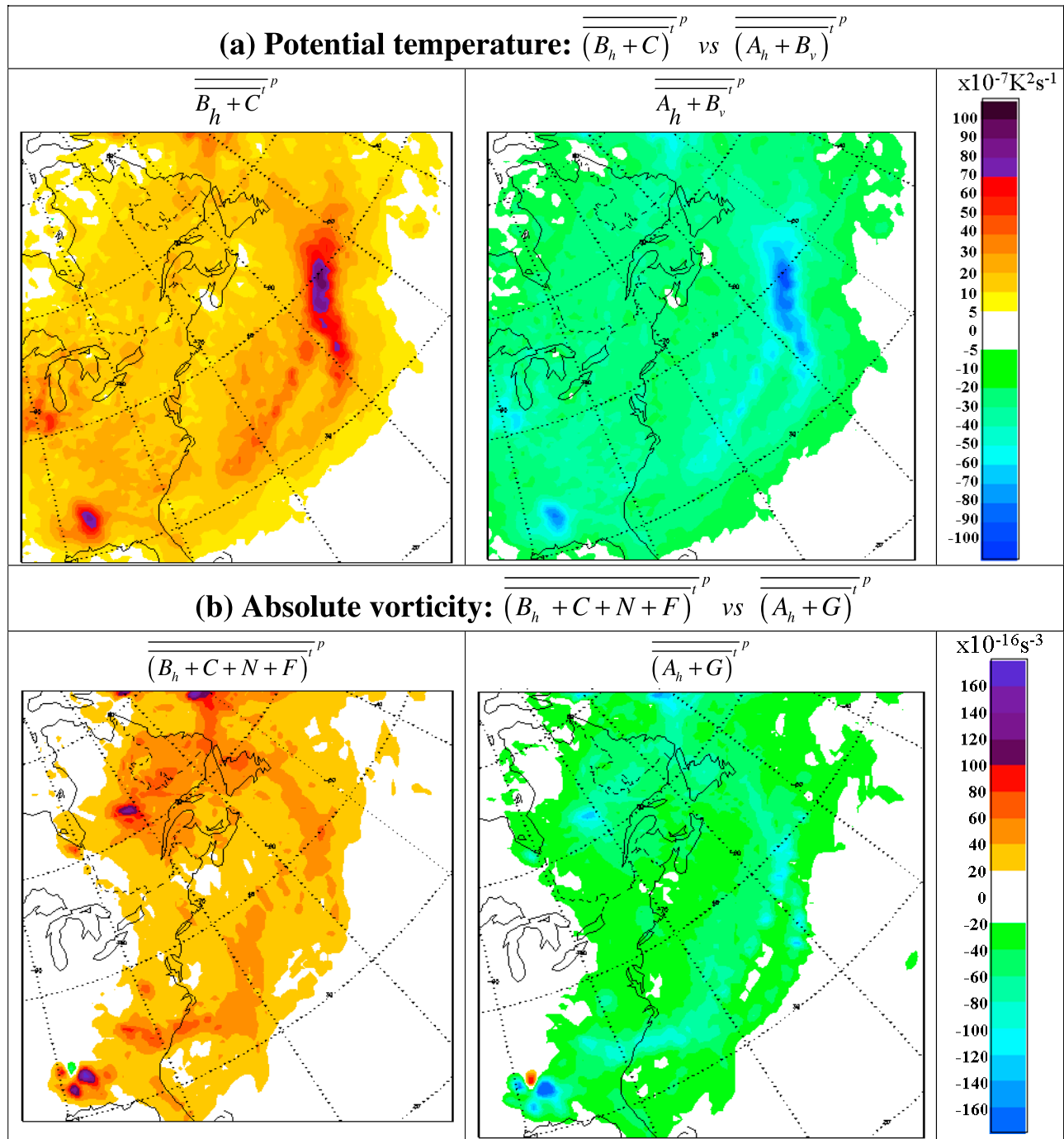


Figure 12. Vertical integral over the whole troposphere of the time average of the sums of source and sink terms in the intermember variance equation for (a) potential temperature and (b) absolute vorticity.

two parts of F (not shown). The positive contributions to the time average of the absolute vorticity IV tendency are balanced by two negative contributions: G and A_h (Figure 11). The first one is the most important, due mainly to the horizontal diffusion (third term of G expression in equation (8)). As mentioned in the case of the potential temperature IV, A_h is a sink term because of the transport of the IV by the ensemble mean flow out of the regional domain.

[39] Figure 12 presents the corresponding fields of the sum of dominant source and sink terms in the troposphere for the two studied variables. Aside from the opposite sign that indicates the nature (source or sink) of the sum, we note good qualitative agreement between source and sink patterns at the seasonal scale. To illustrate the correspondence between them and to get a more quantitative assessment, we present dispersion diagrams in Figure 13 using all grid points shown in Figure 12, and we also compute correlation

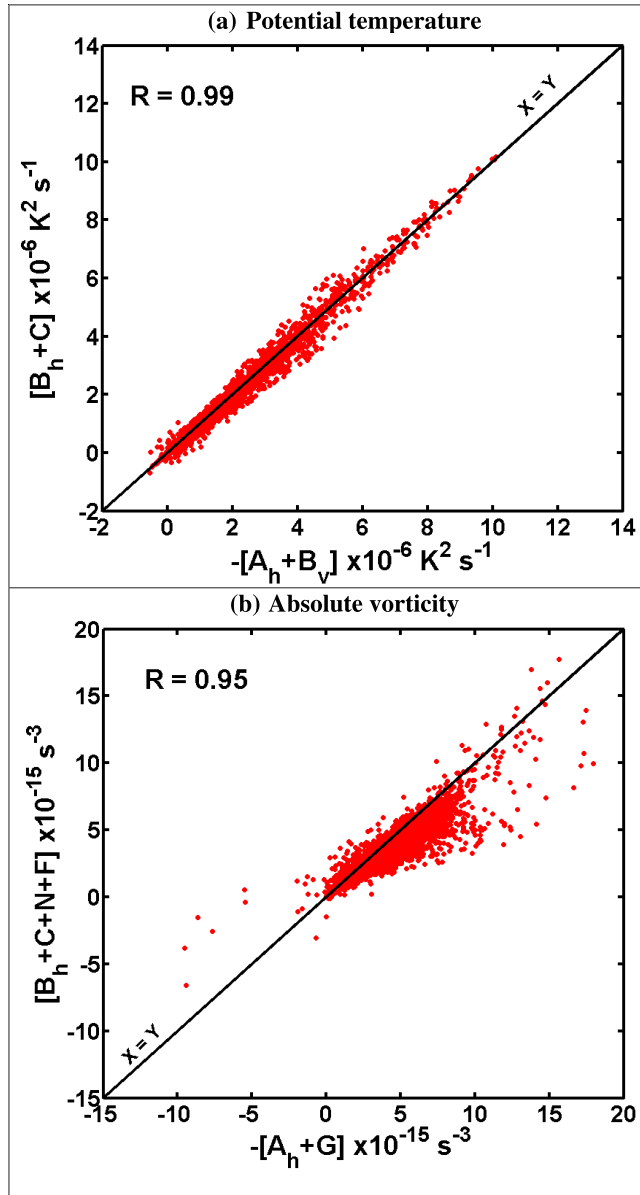


Figure 13. Dispersion diagram of all grid points (except the sponge zone) to illustrate the comparison between sums of source and sink terms in the variance equation for the (a) potential temperature and (b) absolute vorticity.

coefficients. For the potential temperature, the correlation coefficient is about 99%, indicating an excellent balance between the dominant source $\overline{B_h + C}$ and the sink $\overline{A_h + B_v}$ terms at the seasonal scale. In the troposphere, we note the same good correlation (95%) for the absolute vorticity IV, indicating also an approximate balance between four production terms (B_h , C , F and N) and two destruction terms (A_h and G).

4. Summary and Conclusion

[40] We analyzed the physical processes responsible for the maintenance and variations of internal variability (IV) in an ensemble of 20 simulations performed with the nested

Canadian RCM (CRCM) for the summer 1993 season over northeastern North America. The IV is computed as the intermember spread in an ensemble of simulations that differ only in their initiation time. For the two studied variables (potential temperature and absolute vorticity), results show a strong relationship between their time evolutions, and the horizontal patterns of the time-averaged and vertically averaged IV are similar for the two studied variables. These results confirm previous studies indicating that the IV is tied to synoptic conditions [Alexandru *et al.*, 2007; NL10]. We noted that the seasonal mean IV is an order of magnitude smaller than the transient-eddy variability (TE) in simulations; however they have similar vertical profile in the troposphere, with maximum amplitude near the ground and the tropopause, and minimum values in the middle troposphere. The difference in their magnitude is due to the lateral boundary forcing that limits the degrees of freedom in the RCM simulations, at least at the large scales. The control exerted by LBC contributes to generally maintaining IV's magnitude below the value prevailing in GCM simulations, for which IV is equal to TE on average (which is called the ergodicity condition).

[41] The analysis of the magnitude order for the 1993 summer “climatology” of different terms in IV budget equations revealed that the time average of the IV tendency terms are close to zero for the two studied variables. The same result is noted for the sum of all contributions to the seasonal IV tendency, indicating a near equality between the IV generation and destruction contributions, in the time average. Even though the IV fluctuates with synoptic events in the simulations, the vanishing value of the seasonal mean IV tendencies means that there is no trend in IV at the seasonal scale, due to an approximate balance between the four main terms for the potential temperature and the six main terms for the absolute vorticity IV budget equations. Detailed results of vertical profiles and time evolutions of various contributions to IV budget indicate that main terms contribute systematically either positively or negatively in most of the troposphere and in time.

[42] At the seasonal time scale, results showed that the absence of IV trend is due to an approximate balance between terms on average in the troposphere. The time mean IV budget for the potential temperature can be expressed as the following approximate balance:

$$B_h + C \approx -(B_v + A_h) \quad (9)$$

where

$$B_h = -2 \langle \theta'_n \vec{V}'_n \rangle \cdot \vec{\nabla} \langle \theta \rangle; \quad C = 2 \langle \theta'_n J'_n \rangle;$$

$$A_h = -\vec{\nabla} \cdot \left(\langle \vec{V}' \rangle \sigma_\theta^2 \right); \quad B_v = -2 \langle \theta'_n \omega'_n \rangle \frac{\partial \langle \theta \rangle}{\partial p}$$

[43] For absolute vorticity, the balance equation can be approximated as:

$$B_h + C + N + F \approx -(A_h + G) \quad (10)$$

where

$$\begin{aligned}
 B_h &= -2 \langle \eta'_n \vec{V}'_n \rangle \bullet \vec{\nabla} \langle \eta \rangle; & C &= -2 \langle \eta \rangle \langle \eta'_n \vec{\nabla} \bullet \vec{V}'_n \rangle; \\
 N &= -2 \sigma_n^2 \vec{\nabla} \bullet \langle \vec{V}' \rangle \\
 F &= 2S \left[\left\langle \eta'_n \frac{\partial \omega'_n}{\partial Y} \right\rangle \frac{\partial \langle U \rangle}{\partial p} - \left\langle \eta'_n \frac{\partial \omega'_n}{\partial X} \right\rangle \frac{\partial \langle V \rangle}{\partial p} \right]; \\
 A_h &= -\vec{\nabla} \bullet \left(\sigma_n^2 \langle \vec{V}' \rangle \right); & G &= 2S \left[\left\langle \eta'_n \frac{\partial F_{Yn'}}{\partial X} \right\rangle - \left\langle \eta'_n \frac{\partial F_{Xn'}}{\partial Y} \right\rangle \right] \\
 & & & - 2c \langle \eta'_n \nabla^4 \eta'_n \rangle.
 \end{aligned}$$

[44] In these two equations, IV generation and destruction terms are on the left- and right-hand sides, respectively. For both studied variables, B_h and A_h act as positive and negative contributions to the IV tendency, respectively, although they are not the most important contributions. The first one contributes to the IV growth because the transport of heat or positive relative vorticity by covariance of fluctuations is down the gradient in the ensemble mean state. Physically, the second (A_h) is a sink term because of its contribution to transport large IV values out of the regional domain by the horizontal ensemble mean flow.

[45] For the IV budget equation of the potential temperature, the most positive contribution term is C due mostly to the convection and condensation contributions to J . Radiation processes slightly contribute to increase IV in RCM simulations, whereas the vertical and horizontal diffusions act as destruction terms during the season. The most negative contribution to the potential temperature IV is B_v because the time average of the covariance of fluctuations $\left(\overline{\langle \theta'_n \omega'_n \rangle} \right)$ and the gradient of the ensemble mean potential temperature $\left(\frac{\partial \langle \theta \rangle}{\partial p} \right)$ are negative in the entire troposphere. These results reveal that warm fluctuations rise and cold fluctuations sink in perturbations from the ensemble mean state in order to consume IV. Thus the energy conversions associated to IV perturbations appear to behave quite similarly to those in weather systems, with fluctuation available potential energy being generated by condensation and convection processes (term C), and this energy being converted back to fluctuation kinetic energy [e.g., Lorenz, 1955, 1967].

[46] For absolute vorticity, C is a production term because the covariance of fluctuation $\left(\overline{\langle \eta'_n \vec{\nabla} \bullet \vec{V}'_n \rangle} \right)$ is negative indicating that positive (negative) perturbations of the absolute vorticity are associated with the convergence (divergence) of the horizontal flow perturbations. Similarly, the positive contribution of term N is associated with the convergence of the ensemble mean flow of the absolute vorticity. The term F contributes slightly to increase the seasonal IV because the two parts of its expression are positive, according to results. Otherwise, all positive contributions to the absolute vorticity IV are mostly destroyed by the dissipation term G , resulting mainly from the horizontal diffusion (last term in G 's expression).

[47] Our results indicate that RCM's internal variability is a natural phenomenon issued from the chaotic nature of the atmosphere, not a numerical artifact associated, for example,

to the nesting technique. In fact the chaotic nature of the field equations and the ensuing internal variability in ensemble simulations can be advantageously exploited in climate projections. Ensemble simulations are quite useful to filter out the unpredictable component of the Earth System, to provide estimates of the uncertainties associated with climate change projections, and to improve the determination of rare events such as climate extremes.

[48] **Acknowledgments.** This research was done as a project within the Canadian Regional Climate Modeling and Diagnostic (CRCMD) Network at UQAM, which is financially supported by the Canadian Foundation for Climate and Atmospheric Science (CFCAS), the Ouranos Consortium, Hydro-Québec, the Natural Sciences and Engineering Research Council of Canada (NSERC), and the Ministère du Développement Économique, de l'Innovation et de l'Exportation (MDEIE) of the Québec Government. The authors are indebted to G. J. Boer (CCCma) for suggesting the diagnostic methodology. We would like to thank Mourad Labassi, Abderrahim Khaled, and Georges Huard for maintaining user-friendly local computing facility and Adelina Alexandru for allowing us to use her simulated data.

References

- Alexandru, A., R. de Elía, and R. Laprise (2007), Internal variability in regional climate downscaling at the seasonal scale, *Mon. Weather Rev.*, *135*, 3221–3238, doi:10.1175/MWR3456.1.
- Caya, D., and S. Biner (2004), Internal variability of RCM simulations over an annual cycle, *Clim. Dyn.*, *22*, 33–46, doi:10.1007/s00382-003-0360-2.
- Christensen, O. B., M. A. Gaertner, J. A. Prego, and J. Polcher (2001), Internal variability of regional climate models, *Clim. Dyn.*, *17*, 875–887, doi:10.1007/s003820100154.
- de Elía, R., D. Caya, H. Côté, A. Frigon, S. Biner, M. Giguère, D. Paquin, R. Harvey, and D. Plummer (2008), Evaluation of uncertainties in the RCM-simulated North American climate, *Clim. Dyn.*, *30*, 113–132, doi:10.1007/s00382-007-0288-z.
- Giorgi, F., and X. Bi (2000), A study of internal variability of regional climate model, *J. Geophys. Res.*, *105*, 29,503–29,521, doi:10.1029/2000JD900269.
- Laprise, R., D. Caya, M. Giguère, G. Bergeron, H. Côté, J.-P. Blanchet, G. J. Boer, and N. A. McFarlane (1998), Climate and climate change in western Canada as simulated by the Canadian Regional Climate Model, *Atmos. Ocean*, *36*, 119–167.
- Lorenz, E. N. (1955), Available potential energy and the maintenance of the general circulation, *Tellus*, *7*, 157–167, doi:10.1111/j.2153-3490.1955.tb01148.x.
- Lorenz, E. N. (1967), *The Nature and Theory of the General Circulation of the Atmosphere*, 161 pp., World Meteorol. Org., Geneva, Switzerland.
- Lucas-Picher, P., D. Caya, and S. Biner (2004), RCM's internal variability as function of domain size: Research activities in atmospheric and oceanic modelling, *WMO/TD 1220 Rep. 34*, pp. 7.27–7.28, World Meteorol. Org., Geneva, Switzerland.
- Lucas-Picher, P., D. Caya, R. de Elía, and R. Laprise (2008), Investigation of regional climate models' internal variability with a ten-member ensemble of ten-year simulations over a large domain, *Clim. Dyn.*, *31*, 927–940, doi:10.1007/s00382-008-0384-8.
- Nikiéma, O., and R. Laprise (2010), Diagnostic budget study of the internal variability in ensemble simulations of the Canadian RCM, *Clim. Dyn.*, *36*, 2313–2337, doi:10.1007/s00382-010-0834-y.
- Rinke, A., and K. Dethloff (2000), On the sensitivity of a regional Arctic climate model to initial and boundary conditions, *Clim. Res.*, *14*, 101–113, doi:10.3354/cr014101.
- Rinke, A., P. Marbaix, and K. Dethloff (2004), Internal variability in Arctic regional climate simulations: Case study for the Sheba year, *Clim. Res.*, *27*, 197–209, doi:10.3354/cr027197.
- Weisse, R., H. Heyen, and H. von Storch (2000), Sensitivity of a regional atmospheric model to a sea state dependent roughness and the need of ensemble calculations, *Mon. Weather Rev.*, *128*, 3631–3642, doi:10.1175/1520-0493(2000)128<3631:SOARAM>2.0.CO;2.

R. Laprise and O. Nikiéma, Centre Étude et Simulation du Climat à l'Échelle Régionale, Département des Sciences de la Terre et de l'Atmosphère, Université du Québec à Montréal, BP 8888, Stn Downtown, Montréal, QC H3C 3P8, Canada. (nikiema@sca.uqam.ca)